Kinetics of the brominated alkyl radical (CHBr2, CH3CHBr) reactions with NO2 in the temperature range 250–480 K

ARTICLE *in* INTERNATIONAL JOURNAL OF CHEMICAL KINETICS · DECEMBER 2012

Impact Factor: 1.52 · DOI: 10.1002/kin.20725

3 AUTHORS:

Matti Rissanen
University of Helsinki
39 PUBLICATIONS **334** CITATIONS
SEE PROFILE

Arkke J Eskola
University of Helsinki
36 PUBLICATIONS **509** CITATIONS
SEE PROFILE

Raimo S Timonen
University of Helsinki
51 PUBLICATIONS **1,027** CITATIONS
SEE PROFILE

Kinetics of the Brominated Alkyl Radical ($CHBr_2$, CH_3CHBr) Reactions with NO_2 in the Temperature Range 250–480 K

MATTI P. RISSANEN, ARKKE J. ESKOLA, RAIMO S. TIMONEN

Laboratory of Physical Chemistry, Department of Chemistry, University of Helsinki, FIN-00014 Helsinki, Finland

Received 22 September 2011; revised 24 January 2012; accepted 2 February 2012

DOI 10.1002/kin.20725
Published online 29 April 2012 in Wiley Online Library (wileyonlinelibrary.com).

ABSTRACT: The gas-phase kinetics of $CHBr_2 + NO_2$ and $CH_3CHBr + NO_2$ reactions have been studied in direct time resolved measurements using a tubular flow reactor coupled to a photoionization mass spectrometer. The radicals were generated by pulsed laser photolysis of bromoform and 1,1-dibromoethane at 248 nm. The subsequent decays of the radical concentrations were monitored as a function of $[NO_2]$ under pseudo–first-order conditions. The rate coefficients of both reactions are independent of bath gas (He) pressure and display negative temperature dependence under the conditions of 2–6 Torr pressure (He) and 250–480 K. The obtained bimolecular rate coefficients are $k(CHBr_2 + NO_2) = (9.8 \pm 0.4) \times 10^{-12}$ $(T/300\ K)^{-1.65\pm0.18}$ $cm^3\ s^{-1}$ (288–483 K) and $k(CH_3CHBr + NO_2) = (2.27 \pm 0.06) \times 10^{-11}$ $(T/300\ K)^{-1.28\pm0.11}$ $cm^3\ s^{-1}$ (250–483 K), with the uncertainties given as one standard error. Estimated overall uncertainties in the measured bimolecular reaction rate coefficients are ±25%. The reaction products identified were CBr_2O for the $CHBr_2 + NO_2$ reaction and CHBrO and CH_3CHO with minor amounts of CH_3 for the $CH_3CHBr + NO_2$ reaction, respectively.
 Int J Chem Kinet 44: 767–777, 2012

INTRODUCTION

Polybromomethanes are found in considerable quantities over marine environments and coastal areas. They mainly originate from algal production, with substantial additional amounts attributable to human activities [1–9]. At ground level, bromoform ($CHBr_3$) frequently carries more bromine than all the other organobromine compounds together [1,10]. In contrast to its abundance, the amount of direct kinetic studies performed with bromoform's primary photolysis product, $CHBr_2$ radical, are very sparse, constituting only two papers describing the kinetics of the reactions with O_2 and NO [11] and with HBr [12]. The aim of the present paper is to broaden this data set and also to continue our attempts to extract the factors affecting the reactivity between carbon-centered free radicals and NO_2.

To date there have been several direct kinetic measurements of halogen-substituted, carbon-centered free

Correspondence to: Raimo S. Timonen; e-mail: raimo.timonen@helsinki.fi.

radical reactions with NO_2. Eskola and coworkers [13–16] previously measured the rate coefficients of selected R + NO_2 reactions (R = CH_2Cl, CH_2I, CH_2Br, $CHCl_2$, CHBrCl, CCl_2, CCl_3, CH_3CHCl, and CH_3CCl_2). All of these are exothermic, generally fast reactions that show no pressure dependence in the few Torr buffer gas pressure range, display negative temperature dependence and thus appear to proceed from reactants to products without an activation barrier. Other halogenated alkyl radical reactions with NO_2 subject to direct studies include the relatively widely explored CF_3 + NO_2 reaction, most recently studied by Breheny et al. [17] with IR spectrometry (see [17] and references there in) and CF_2Cl + NO_2 reaction investigated by Slagle and Gutman [18] using photoionization mass spectrometry. Temperature dependencies have been obtained for the reactions measured by Eskola et al. [13–16] and for the mentioned CF_3 + NO_2 reaction [17].

In the present study, we describe the first direct measurements of the rate coefficients of two brominated radical reactions:

$$CHBr_2 + NO_2 \rightarrow \text{Products} \quad (1)$$

$$CH_3CHBr + NO_2 \rightarrow \text{Products} \quad (2)$$

Possible reaction pathways based on observed products are discussed, and the reactivity of the radicals is briefly compared with other previously studied R + NO_2 reactions.

EXPERIMENTAL

Details of the experimental apparatus and procedures have been described previously [19,20], so only a summary is given here. The gas mixture flowing through a reactor contained the radical precursor (<0.02%), NO_2 in varying amounts and an inert carrier gas (He) in large excess (>99.7%). The brominated radicals were homogeneously generated along the tubular flow reactor by a pulsed, unfocused KrF (248 nm) exciplex laser (ELI-76) photolysis of bromoform ($CHBr_3$) and 1,1-dibromoethane (CH_3CHBr_2). Output fluence of the photolysing pulse was measured (Gentec ED-200) in each experiment and was typically between 10 and 25 mJ cm^{-2}. The laser was operated with a 5-Hz repetition rate, and the gas flow velocity through the tubular temperature controlled region of the reactor was held at about 5 ms^{-1}. This ensured that the gas flowing through the reaction volume was always completely replaced between laser pulses. The reactor tube used in measurements was made of seamless stainless steel with an 8-mm inner diameter and was coated with halocarbon wax (HW) or polydimethylsiloxane (PDMS).

The reaction gas mixture was continuously sampled through a small hole (0.4 mm i.d.) in the wall of the reactor and formed into a beam by a conical skimmer in the entrance of the vacuum chamber containing the photoionization mass spectrometer. As the gas beam traversed the ion source, a portion of molecules was photoionized with a resonance lamp and the ions formed were mass selected in a quadropole mass spectrometer (Extrel, C-50/150-QC/19 mm rods). Mass-selected ion signals were recorded with a multichannel scaler (EG&G Ortec MCS plus) from 10 ms before the laser pulse to up to 80 ms after it. Data from 3000 to 25,000 laser pulses were accumulated, and the nonlinear least-squares method was used to fit an exponential function $[R]_t = [R]_0 \times \exp(-k't)$ to the acquired data. Parameters $[R]_0$ and $[R]_t$ are the signals proportional to the radical concentration promptly after the laser pulse and at time t, and k' is the first-order rate coefficient.

All experiments were conducted under conditions where the molecular reactant was in large excess so that only two significant processes consumed the radicals in the reactor: reaction with NO_2 and the first-order heterogeneous loss on the walls of the reactor. This ensured that the results obtained showed pseudo–first-order kinetics, and the bimolecular rate coefficients for reactions (1) and (2) could be obtained from the slopes of the plots of k' against $[NO_2]$. A typical example of this procedure is shown in Fig. 1 for the $CHBr_2$ + NO_2 reaction. The insets in Fig. 1 display an example of a $CHBr_2$ radical decay observed in the measurements together with the corresponding formation profile of CBr_2O product. Figure 2 displays a similar plot for the CH_3CHBr + NO_2 reaction.

At the beginning and at the end of each experiment, the wall loss rate (k_w) was determined in the absence of NO_2 (i.e., k' when $[NO_2] = 0$). Radical precursor concentrations were reduced until the observed wall loss rate did not depend on the concentration and an exponential fit to the radical signal showed no deviation from the first-order decay. Once this was accomplished, it was presumed that all radical–radical and radical–atom reactions occurring in our system had negligible rates compared with the first-order reactions under study.

The $CHBr_2$ radicals were generated in the photolysis of $CHBr_3$, where the possible dissociation pathways following single photon absorption at 248 nm are [21]

$$CHBr_3 + h\nu\ (248\ \text{nm}) \rightarrow CHBr_2 + Br \quad (3a)$$

$$\rightarrow CHBr + Br_2 \quad (3b)$$

$$\rightarrow CBr_2 + HBr \quad (3c)$$

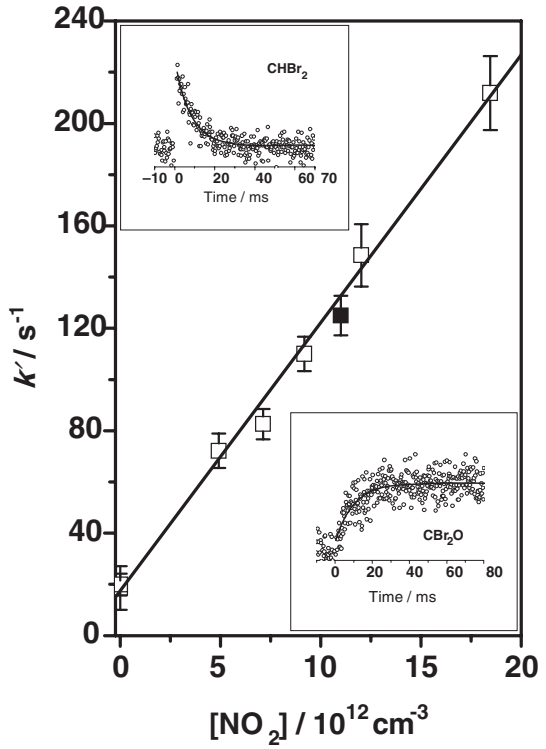

Figure 1 A typical plot of the measured pseudo–first-order rate coefficients k' as a function of $[NO_2]$ for a set of experiments conducted to determine the bimolecular rate coefficient of the $CHBr_2 + NO_2$ reaction at 298 K and 5.2 Torr He. The upper inset is an ion signal profile observed for the $CHBr_2$ radical decay, from which k' was obtained, and the lower inset shows the concomitant product formation profile of CBr_2O. The ion signals were recorded under the conditions of the solid square in the plot: $[NO_2] = 1.1 \times 10^{13}$ cm^{-3}, $[He] = 1.7 \times 10^{17}$ cm^{-3}. The first-order exponential fits to the signals gave decay and formation coefficients: k'_d ($CHBr_2$, $m/z = 173$) $= 125 \pm 7$ s^{-1}, k'_f (CBr_2O, $m/z = 186$) $= 107 \pm 8$ s^{-1}, where uncertainties are one standard deviation (1σ).

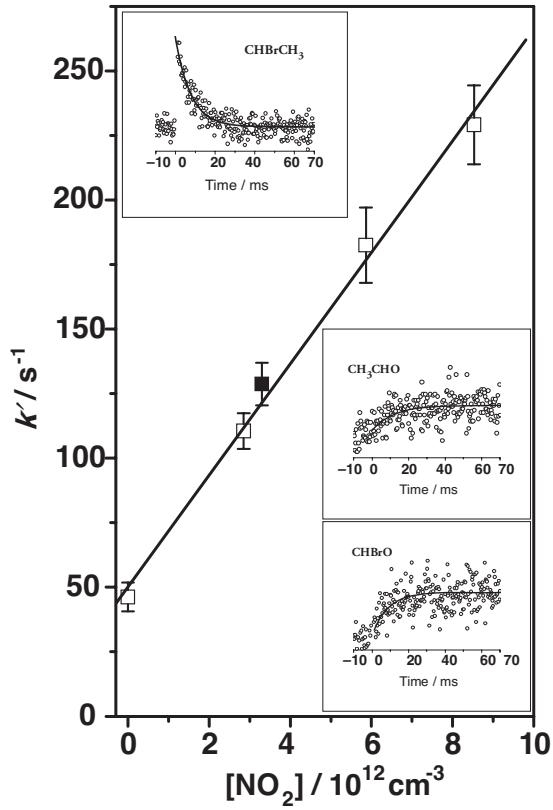

Figure 2 A plot of the pseudo–first-order rate coefficients (k') against $[NO_2]$ of the $CH_3CHBr + NO_2$ reaction at 298 K and 6.0 Torr He. The ion signal profiles shown in insets were recorded under the conditions of the solid square in the plot: $[NO_2] = 3.3 \times 10^{12}$ cm^{-3}, $[He] = 1.9 \times 10^{17}$ cm^{-3}. The lines drawn through the data in the insets are first-order exponential fits, with decay and formation coefficients: $k'_d(CH_3CHBr, m/z = 107) = 131 \pm 8$ s^{-1}, $k'_f(CHBrO, m/z = 108) = 114 \pm 16$ s^{-1}, and $k'_f(CH_3CHO, m/z = 44) = 88 \pm 18$ s^{-1}.

The channel (3a) has been described as the almost exclusive reaction pathway of photolysis of $CHBr_3$ at 248 nm [21].

The photodissociation of CH_3CHBr_2, was used to produce the CH_3CHBr radicals [22]:

$$CH_3CHBr_2 + h\nu\ (248\ \text{nm}) \rightarrow CH_3CHBr + Br \quad (4a)$$

$$\rightarrow \text{Other products} \quad (4b)$$

Initial $CHBr_2$ radical concentrations in the experiments were estimated from the known absorption cross section of bromoform [21], laser intensity, and concentration of the precursor in the gas flow. Because the absorption cross section for CH_3CHBr_2 is not available, we estimated the initial CH_3CHBr radical concentrations from the precursor decomposition signal; the depletion of the CH_3CHBr_2 signal due to the laser pulse photolysing the gas mixture. Initial radical concentrations were determined to be between 0.8×10^{11} and 4×10^{11} cm^{-3} in all measurements. NO_2 concentrations were measured by a pressure change in a calibrated volume method and were corrected for dimerization, as described below.

The resonance lamps used in the study to seek and detect radicals and products were a Cl-lamp (8.9–9.1 eV) for $CHBr_2$, CH_3CHBr, and HCO; a H lamp (10.2 eV) for $CHBr_2$, CH_3CHBr, CH_3CHBrO, $CH_3CHBrNO_2$, $CHBr_2NO_2$, CBr_2NO, $CHBr_2O$, $CHBrO$, CBr_2, CBr_2O, $CHBr$, $BrNO_2$, $BrNO$, BrO, CH_3CHO, CH_3CH, CH_3, HCO, HNO_2,

Table I Results and Conditions of the Experiments Used to Measure Rate Coefficients of Reactions R + NO_2 → Products (R = $CHBr_2$ and CH_3CHBr)[a]

T/(K)	[He]/(10^{17} cm^{-3})	[NO_2]/(10^{12} cm^{-3})	k/(10^{-12} cm^3 s^{-1})[b]	Reactor Coating	k_{wall} /(s^{-1})
		R = $CHBr_2$, ($CHBr_2$ + NO_2 → Products)			
		$k(CHBr_2 + NO_2) = (9.8 \pm 0.4) \times 10^{-12}$ $(T/300\ K)^{-1.65\pm0.18}$ cm^3 s^{-1}			
288	0.80	2.0–19.6	10.4 ± 0.80	HW	12
288	1.61	1.9–18.4	10.9 ± 0.65	HW	19
288	1.98	2.0–14.6	10.1 ± 0.12	HW	19
298[c,d]	1.62	4.9–18.5	10.5 ± 0.33	HW	19
338	1.60	2.2–22.1	8.76 ± 0.60	HW	8
363	1.57	4.2–26.5	5.94 ± 0.45	HW	10
383[c]	1.59	6.4–32.0	6.30 ± 0.44	PDMS	52
433[e]	1.61	6.9–33.6	6.04 ± 0.44	PDMS	57
483[c,d]	1.46	5.8–38.5	4.38 ± 0.34	PDMS	57
		R = CH_3CHBr, (CH_3CHBr + NO_2 → Products)			
		$k(CH_3CHBr + NO_2) = (2.27 \pm 0.06) \times 10^{-11}$ $(T/300\ K)^{-1.28\pm0.11}$ cm^3 s^{-1}			
250	1.85	2.8–8.5	26.6 ± 2.89	HW	58
267	1.74	2.2–5.1	29.4 ± 1.46	HW	74
298	0.78	1.8–8.7	24.5 ± 3.27	HW	33
298[e]	1.62	2.0–13.5	21.7 ± 2.21	HW	60
298	1.69	4.6–11.8	22.3 ± 2.03	HW	50
298[c,d]	1.94	2.8–8.5	21.6 ± 0.89	HW	46
336	1.58	2.5–9.8	19.3 ± 1.24	HW	47
393[c,d]	1.45	2.0–8.4	17.4 ± 1.11	PDMS	70
433	1.38	2.0–10.2	14.6 ± 0.39	PDMS	72
483[e]	1.36	2.3–13.3	11.5 ± 1.70	PDMS	63

Estimated overall uncertainties in the measured bimolecular reaction rate coefficients are ±25%. Abbreviations: HW, halocarbon wax; PDMS, polydimethylsiloxane.

[a] Range of precursor concentrations used: (3–10) × 10^{12} cm^{-3} for $CHBr_3$ and (1.6–4.4) × 10^{13} cm^{-3} for CH_3CHBr_2.

[b] Statistical uncertainties shown are one standard error.

[c] Estimated initial radical concentration was under 1 × 10^{11} cm^{-3}. In all the other experiments, the estimated initial radical concentration was under 4 × 10^{11} cm^{-3}.

[d] Experiments performed with low laser power (E_p ≈ 6–10 mJ cm^{-2}) and low precursor concentration ([$CHBr_3$] ≈ (3–5) × 10^{12} cm^{-3}, [CH_3CHBr_2] ≈ (1.6–2.2) × 10^{13} cm^{-3}).

[e] Experiments performed with high laser power (E_p ≈ 20–25 mJ cm^{-2}) and high precursor concentration ([$CHBr_3$] ≈ 10^{13} cm^{-3}, [CH_3CHBr_2] ≈ (3.4–4) ×10^{13} cm^{-3}).

HNO, and NO; and a Ne-lamp (16.7 and 16.9 eV) for $CHBr_2NO_2$, $CHBr_2NO$, CBr_2O, $CHBrOCH_3$ CHBrO, CH_3CHOBr_2, BrO, $BrNO_2$, BrNO, HBr, Br, HNO, HNO_2, and CO. All the kinetics were measured with a chlorine lamp. However, a few radical decay profiles were obtained using a hydrogen lamp for comparison. No differences, other than change in the signal intensity and background level were observed.

Radical precursors, CH_3CHBr_2 (Acros Organics; purity 99%) and $CHBr_3$ (Merck; purity 96%) were degassed by several freeze–pump–thaw cycles before use. The NO_2 gas (Merck; purity 98%) was diluted in helium to form a 6%–12% mixture and was stored in and used from a blackened Pyrex bulb. Helium (Messer-Griesheim; purity 99.9996%) was employed as supplied.

RESULTS AND DISCUSSION

The results and conditions of the rate coefficient measurements are presented in Table I. The stated uncertainties are statistical one standard error obtained from fits to the experimental data. The estimated overall uncertainty in the measured bimolecular rate coefficients is about ±25%, which was estimated from uncertainties in determined NO_2 concentrations and uncertainties in the measured pseudo–first-order rate coefficients. The NO_2 concentrations were determined with the pressure increase in a known volume method and thus contain uncertainties from the calibration of the known volume, measurements of the time the pressure increased in this volume, the uncertainties of the measured main gas flow velocities and pressures, and in addition, the uncertainty of the purity of the prepared

NO_2 gas mixture. The uncertainties of the fitting of the pseudo–first-order rate coefficients to the decaying radical signals mainly resulted from the random noise in the measured temporal signals (see Figs. 1 and 2).

In calculating the reactant concentrations, attention has to be paid to the dimerization of NO_2 to N_2O_4 in the storage bulb and its decomposition back to NO_2 in the reactant flow. The unimolecular decomposition [23,24] rate of N_2O_4 is about 1000 s^{-1} under the conditions under which the reactant flow rates were measured (about 8 Torr and 298 K). Owing to the rapid conversion of dimers to monomers compared with the rather long residence time in a measuring volume (flow from a high p source bulb to a low p measuring volume), the conversion from concentrated to dilute gas happens fast. According to equilibrium thermodynamics [25], about 31% (depending on the used concentration) of NO_2 is in the form of N_2O_4 in the source bulb. This fraction decreases to about 1% in the measuring volume and is below 0.1%, at the reactor inlet. Such a small amount of N_2O_4 in the reaction mixture is of no concern, even though N_2O_4 has a larger absorption coefficient than NO_2 at 248 nm [23]. Photolysis of N_2O_4 at this wavelength produces only NO_2 molecules in various excited states, which are quenched within the first millisecond after the photolysing laser pulse. The first millisecond of the radical decay signal is always omitted from the analysis of the first-order exponential decay rate to ensure that only kinetics of thermalized species are observed. Hence only the fraction of NO_2 that is in the form of N_2O_4 in the source bulb, in addition to the total $p(NO_2, N_2O_4)$, is needed for the reactant concentration calculations and is calculated using equilibrium thermodynamics [25].

Photodissociation of NO_2 at 248 nm [23], which produces ground state oxygen atoms and NO in the system, could be a source of problems in the rate determinations. In this case, the possible problems could include (i) production of the measured radicals in chain reactions with O-atoms and precursor molecules, effectively decreasing the observed first-order rate coefficients; (ii) enhancement of the determined rate coefficients when NO and O are reacting with the measured radicals; or (iii) lowering of the concentration of available NO_2 molecules resulting in decreased rate coefficients. Typical initial oxygen atom and NO concentrations were between 1×10^{10} and 2×10^{10} cm^{-3} and never above 3.5×10^{10} cm^{-3} and were estimated from the measured laser intensities and absorption cross section of NO_2 [23]. This small amount of O-atoms/NO-molecules cannot cause any of the problems (i)–(iii) presented above, as the low O-atom and NO-molecule concentrations are effectively scavenged by the photolytic precursors ($CHBr_3$ and CH_3CHBr_2) and NO_2, which are all the time in great excess over radical concentrations. This was verified by performing simulations of the current reaction system. The simulations showed that, for example, the lifetime of O-atoms in the system is in the order of half a millisecond or less by considering the fast reactions of $CHBr_3 + O$ and $NO_2 + O$ only, which are all the time present in the $CHBr_2 + NO_2$ experiments ($k(CHBr_3 + O) = 6.6 \times 10^{-10}$ cm^3 s^{-1} and $k(NO_2 + O) = 1.04 \times 10^{-11}$ cm^3 s^{-1}) [23].

The usable temperature range in the experiments was extended by applying two different reactor tube coating materials. When PDMS was used as a reactor coating, the observed first-order wall loss rates were higher than when using HW coating (Table I). Otherwise, the obtained results are consistent with each other and the determined bimolecular rate coefficients fitted to the same temperature dependency for both used coating materials (see Fig. 3). Measurements of the $CHBr_2 + NO_2$ reaction rate coefficients were not continued below 288 K due to the instability of the observed $CHBr_2$ radical wall loss rates, that is $k_w(CHBr_2)$ became much higher and irregular at temperatures lower than $T =$ 288 K and the experiments were discontinued (according to the NIST recommendation [26] $T_{fus}(CHBr_3) = 279 \pm 10$ K with six different determinations; see original references from [26]).

Tests were also performed to investigate the rate coefficients dependence on helium bath gas density. The same rate measurements were carried out at nearly three times higher bath gas density without changing the concentration of the reactants. The obtained rate coefficients were the same within statistical uncertainties, suggesting that the title reaction rate coefficients are pressure independent within the experimental range (2–6 Torr).

CBr_2O ($m/z = 186$) was observed as a product of the $CHBr_2 + NO_2$ reaction (Fig. 1). In addition, a weak formation signal attributed to CHBrO ($m/z =$ 108) was detected. An implication that the measured CBr_2O ($m/z = 186$) signal originates from the studied reaction is that it has the same first-order formation rate as the $CHBr_2$ ($m/z = 173$) radical decay obtained from sequential measurements (see Fig. 1). Other potential products that were sought but not detected for the $CHBr_2 + NO_2$ reaction included $CHBr_2NO_2$ (m/z = 217, 219), $CHBr_2NO$ ($m/z = 201$), CBr_2NO ($m/z =$ 200), $CHBr_2O$ ($m/z = 189$, 191), CHBr ($m/z = 92$), $BrNO_2$ ($m/z = 125$), BrNO ($m/z = 109$), BrO ($m/z =$ 95), CHO, CO, HNO_2, and HNO.

According to previous studies of analogous carbon-centered free radical reactions with NO_2 [27–29], the expected products of the $CHBr_2 + NO_2$ reaction

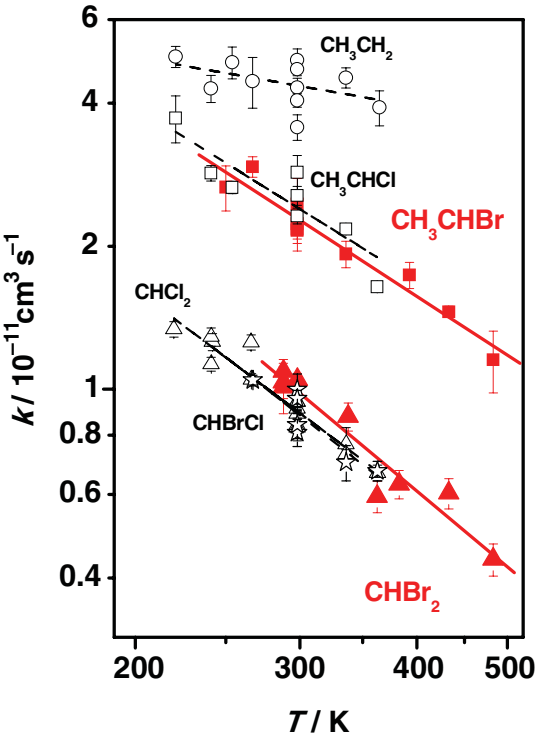

Figure 3 Double-logarithmic plot of the measured bimolecular reaction rate coefficients as a function of T together with selected previously published results. The current results are indicated by filled symbols. The data for $CHCl_2 + NO_2$ reaction [$k = (8.90 \pm 0.16) \times 10^{-12}$ $(T/300\ K)^{-1.48\pm0.13}$] (open triangles) was obtained from [13], for $CHBrCl + NO_2$ reaction [$k = (8.81 \pm 0.28) \times 10^{-12}$ $(T/300\ K)^{-1.55\pm0.34}$] (stars) from [14], for $CH_3CHCl + NO_2$ reaction [$k(CH_3CHCl + NO_2) = (2.38 \pm 0.10) \times 10^{-11}$ $(T/300\ K)^{-1.27\pm0.26}$] (squares), and $CH_3CH_2 + NO_2$ reaction [$k(CH_3CH_2 + NO_2) = (4.33 \pm 0.13) \times 10^{-11}$ $(T/300\ K)^{-0.34\pm0.22}$] (circles) from [16]. Units of the rate coefficients are $cm^3\ s^{-1}$. [Color figure can be viewed in the online issue, which is available at wileyonlinelibrary.com.]

are $CHBr_2ONO$ and $CHBr_2NO_2$. From these, the nitrite product ($CHBr_2ONO$) preferably decomposes to $CHBr_2O$ and NO [27–29] and the formed alkoxy radical ($CHBr_2O$) is expected to promptly dissociate further to CHBrO and Br [11,30–32]. Bayes et al. [11] have postulated that any substituted methoxy radical containing merely one bromine atom will dissociate rapidly, even at atmospheric pressures.

Drougas and Kosmas [32] have investigated the $CHBr_2O$ radical computationally and have calculated the Rice–Ramsperger–Kassel–Marcus rate coefficients for the different unimolecular decomposition channels. They found that although the C—Br bond scission process (5b) is the energetically most favorable pathway, the C—H bond scission (5a) and the formation of CBr_2O prevails in the high-energy region when the total energy of the parent $CHBr_2O$ radical gained from the reaction exceeds about 45 kcal mol^{-1}. If the product $CHBr_2O$ is formed and it is formed with considerable amount of internal excitation (denoted by an asterisk) then the oxygenated products could be explained through the following reaction scheme:

$$CHBr_2 + NO_2 \rightarrow CHBr_2O^* + NO \quad (1a)$$

$$\rightarrow \text{Other products} \quad (1b)$$

$$CHBr_2O^* \rightarrow CBr_2O + H \quad (5a)$$

$$\rightarrow CHBrO + Br \quad (5b)$$

$$\rightarrow \text{Other products.} \quad (5c)$$

However, 45 kcal mol^{-1} is a fairly high excitation and could be produced only in a very exothermic reaction. We examined the thermochemistry of reaction (1a) using the literature [12,32–34] ($\Delta_f H(CHBr_2) = 47.6$ kcal mol^{-1} [12], $\Delta_f H(CHBr_2O) = 21.3$ kcal mol^{-1} [32–34], $\Delta_f H(NO_2) = 7.9$ kcal mol^{-1} [33], and $\Delta_f H(NO) = 21.6$ kcal mol^{-1} [33]) and calculated the exothermicity of the channel (1a) to be about 13 kcal mol^{-1}; clearly too low to explain the observations. Also, it should be pointed out that the reaction thermochemistry calculation is very unlikely uncertain by as much as 30 kcal mol^{-1}.

The assignment of the observed CBr_2O as a product of the $CHBr_2 + NO_2$ reaction could be thought of being problematic because it could have been postulated to form in a $CBr_2 + NO_2$ reaction, if CBr_2 radical was produced in the $CHBr_3$ photolysis (3c). Zou et al. [21] have studied the photolysis of bromoform at 248 nm using vacuum ultraviolet (VUV) ionization photofragment translational spectroscopy. They could not find evidence of significant CBr_2 production, considering also the secondary dissociation processes of $CHBr_2$. Xu et al. [35] have studied the photodissociation of bromoform at 234 and 267 nm by ion velocity imaging and have not observed anything suggesting the formation of the CBr_2 radical. Furthermore, we have not been able to observe any signal that could have been assigned to the CBr_2. This was already thoroughly investigated and discussed by Seetula and Eskola in their $CHBr_2 +$ HBr study [12], where the production of CBr_2 could have had more serious consequences.

There also exists indirect evidence that the observed CBr_2O does not come from the $CBr_2 + NO_2$ reaction. Eskola et al. [15] measured the rate coefficients of the $CCl_2 + NO_2$ reaction resulting in a room temperature value of $k_{300\,K} = 1.76 \times 10^{-13}$ $cm^3\ s^{-1}$. In line with this (see below) and previous studies, the rate coefficients of halogenated carbon-centered free radical reactions with NO_2 are not affected much by substituting Cl

with Br atoms. Taking this into account, the observed CBr_2O formation kinetics are much too fast to be produced in a $CBr_2 + NO_2$ reaction, that is, $k_{300\,K}(CHBr_2 + NO_2)/k_{300\,K}(CCl_2 + NO_2) \approx 9.8 \times 10^{-12}/1.76 \times 10^{-13} \approx 55.7$. Finally, it should be noted that as all of the title reaction (1) kinetics were measured with a chlorine lamp, the CBr_2 ion signal cannot interfere with the measurements, because CBr_2 has an ionization energy (IE) above the energy of the chlorine lamp ($IE(CBr_2) = 10.11$ eV [36]).

The mechanism of the $CHBr_2 + NO_2$ reaction remains unclear. Considering the previous studies and the reasoning presented above, it seems that the observed CBr_2O is very unlikely formed through the $CHBr_2O$ alkoxy radical (reactions (1a) and (5a)). Another possible pathway to product formation is via a four-center transition state; first postulated for the NO_2 reaction by Sugawara et al. [37] in a $CF_3 + NO_2$ reaction and later by us to explain the CH_3CHO formation in the $CH_3CHCl + NO_2$ reaction [16]. The transition state for the $CHBr_2 + NO_2$ reaction (1c) could be composed of a ring with C, O, N, and H atoms:

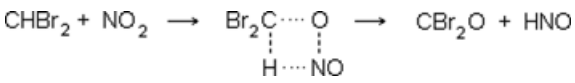

(1c)

which dissociates to CBr_2O and HNO fragments. The HNO formation, despite multiple attempts with different ionization energies, could not be verified in the measurements, probably due to the low detection sensitivity of the apparatus to HNO.

Also another similar type of transition state (1d) can be proposed, with C, O, N, and Br forming the four-center ring structure:

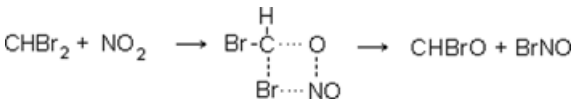

(1d)

It would be interesting to compare the energetics between alkoxy (reactions (1a) and (5a)) and the suggested four-center elimination pathways, but unfortunately energetics for the latter are not available.

Products observed for the $CH_3CHBr + NO_2$ reaction were CHBrO ($m/z = 108$) and CH_3CHO (Fig. 2) with minor amounts of CH_3. The measured ion signal for CH_3 was weak and noisy, and the quality of the signal did not allow a proper fitting to obtain its formation kinetics. Nevertheless, formation of a product with a mass of 15 Da was evident when a H lamp (10.2 eV) was used for ionization. Other potential products that were sought, but not detected included $CH_3CHBrNO_2$ ($m/z = 153$), CH_3CHBrO ($m/z = 123$), BrNO ($m/z = 109$), BrO ($m/z = 95$), CHO, $CHCH_3$, HNO_2, and HNO.

Drougas and Kosmas [38] and Orlando and Tyndall [39] have investigated the unimolecular decomposition of the CH_3CHBrO radical and have found that unlike the HCl elimination from the analogous CH_3CHClO radical [39], the C—Br bond scission and formation of CH_3CHO and Br is much more probable. We could not detect CH_3CHBrO in the product search, but this cannot be taken as a proof of its absence since the alkoxy species are known to be difficult to detect with photoionization using resonance gas lamps in the millisecond time scale [27]. Expected alkoxy radicals were sought in all of the previous $R + NO_2$ studies [13–16,27,40], but the attempts were always unsuccessful. Most likely their detection in the millisecond time window is not possible due to their rapid dissociation caused by internal excitation from the reaction. Another possibility for their absence is photodissociation while attempting ionization, and their successful detection may require a tunable UV source [41] for ionization near the threshold.

If the primary product is CH_3CHBrO and it is formed with substantial internal excitation, then the observed products CH_3CHO, CHBrO, and CH_3 could be formed in a reaction sequence:

$$CH_3CHBr + NO_2 \rightarrow CH_3CHBrO^* + NO \quad (2a)$$

$$\rightarrow \text{Other products} \quad (2b)$$

$$CH_3CHBrO^* \rightarrow CH_3CHO + Br \quad (6a)$$

$$\rightarrow CHBrO + CH_3 \quad (6b)$$

$$\rightarrow \text{Other products.} \quad (6c)$$

The theoretical study by Drougas and Kosmas [38] showed that dissociation routes (6a) and (6b) are the most prominent with associated energy barriers of 1.1 and 11.5 kcal mol^{-1}, respectively. With the literature [12,33,38,42], we were able to calculate the exothermicity of the reaction (2a) ($\Delta_f H(CH_3CHBr) = 31.9$ kcal mol^{-1} [12], $\Delta_f H(CH_3CHBrO) = -3.3$ kcal mol^{-1} [33,38,42], $\Delta_f H(NO_2) = 7.9$ kcal mol^{-1} [33], and $\Delta_f H(NO) = 21.6$ kcal mol^{-1} [33]), resulting in 21 kcal mol^{-1}. Based on the previous studies and on the observed products (CHBrO, CH_3CHO, and CH_3), an internally excited $CH_3CHBrONO$ is expected to be produced in the $CH_3CHBr + NO_2$ reaction. The formed $CH_3CHBrONO$ dissociates rapidly into CH_3CHBrO and NO, and the alkoxy radical (CH_3CHBrO) decomposes further to the observed fragments via reactions (6a) and (6b).

It should be noted, however, that to our knowledge nothing excludes the four-center transition state pathway to be feasible for this reaction too. As mentioned above, we observed CH_3CHO as a primary product in a previous $CH_3CHCl + NO_2$ investigation, in contrast to the expected CH_3CO and HCl products from the alkoxy decomposition channel. If the transition state is similar to the one proposed for the $CH_3CHCl + NO_2$ reaction [16] (and the $CHBr_2 + NO_2$ reaction) then the expected products would be CH_3CHO and BrNO. From these, the latter will most likely dissociate due to internal excitation from the reaction or during photoionization [16]. However, the presence of CH_3 (which can be formed through reaction (6b) and not easily in a ring process) might point to at least a minor involvement of the alkoxy intermediate.

NO was also observed in both of the reactions, but assigning its production to reactions (1a) and (2a) is problematic. Photodissociation of NO_2 produces prompt NO and oxygen atoms to the system. The oxygen atoms will most likely react with present NO_2 to form $NO + O_2$. Also it is possible that some labile products as well as photolysis side-products can react with NO_2, forming more NO in the reaction mixture. Hence, identification of NO as a reaction product is severely hindered by these background signals and cannot be unambiguously shown to be produced in the studied $R + NO_2$ reactions.

The results from current experiments together with selected previously measured rate coefficients are presented in Fig. 3. The solid lines in the figure present linear least-squares fits of an exponential function $k = A \times (T/300\ \mathrm{K})^n$ to the current experimental data. In this equation, T is temperature in Kelvin and A and n are empirical parameters.

The bimolecular rate coefficients of the reactions (1) and (2) have not been measured previously, but they share the common characteristics that have previously been observed for the carbon-centered free radical reactions with NO_2: exothermicity, rapidness, negative temperature dependence, and pressure independence at a few Torr pressure range. It has also been established that halogen substitution at the radical center reduces the reactivity of substituted alkyl radical reactions, because of the electron-withdrawing inductive effect of the electronegative halogen atoms [13,14,16]. Electropositive alkyl substituents have the opposite effect, and they enhance the observed reaction rates. These trends are again observed in the current results (Figs. 3, 4a, and 4b).

In previous experiments [13,14,16], we have measured the bimolecular rate coefficients of the $CHCl_2 + NO_2$, $CHBrCl + NO_2$, and $CH_3CHCl + NO_2$ reactions, which are relevant for comparison with the results obtained in this study. The room temperature rate coefficients obtained in these previous experiments were (in units of $cm^3\ s^{-1}$) $k_{300\,K}(CHCl_2 + NO_2) = (8.90 \pm 0.16) \times 10^{-12}$, $k_{300\,K}(CHBrCl + NO_2) = (8.81 \pm 0.28) \times 10^{-12}$, and $k(CH_3CHCl + NO_2) = (2.38 \pm 0.10) \times 10^{-11}$. It is interesting to notice that there is only a very little difference in the absolute values of the rate coefficients and in the temperature dependencies of the reactions of $CHBr_2$ ($k_{300\,K}(CHBr_2 + NO_2) = (9.8 \pm 0.4) \times 10^{-12}\ cm^3\ s^{-1}$) and the chlorinated analogue $CHCl_2$, as well as the CHBrCl containing both Cl and Br atoms (see Fig. 3). The corresponding temperature dependencies (as noted with the parameter n in the expression $k_{300\,K}(T/300\,K)^n$) are -1.48 ± 0.13, -1.55 ± 0.34, and -1.65 ± 0.18 for the $CHCl_2$, CHBrCl, and $CHBr_2$ reactions with NO_2, respectively. In substituted ethyl radicals, the same behavior is observed already at the monosubstitution level; the bimolecular rate coefficients and the temperature dependencies obtained for the $CH_3CHCl + NO_2$ and $CH_3CHBr + NO_2$ reactions are the same ($k_{300\,K}(CH_3CHBr + NO_2) = (2.27 \pm 0.06) \times 10^{-11}\ (T/300\ K)^{-1.28\pm0.11}\ cm^3\ s^{-1}$ and ($k(CH_3CHCl + NO_2) = (2.38 \pm 0.10) \times 10^{-11}\ (T/300\ K)^{-1.27\pm0.26}\ cm^3\ s^{-1}$) within experimental uncertainties.

Other halogenated alkyl radical reactions with NO_2 relevant to this study include the relatively widely explored $CF_3 + NO_2$ reaction (see [17] and references there in) and $CF_2Cl + NO_2$ reaction. The $CF_3 + NO_2$ reaction has been studied by Breheny et al. [17] over a large pressure range (1.5–110 Torr), but in a relatively narrow temperature range (251–295 K). They used IR spectrometry to detect CF_2O and FNO product formations, which enabled them to extract the kinetics of CF_3 removal by NO_2. No variation of the rate coefficients with buffer gas pressure was observed, which is in accordance with the present study, where no pressure dependencies are seen. They reported a bimolecular reaction rate coefficient $k_{295K}(CF_3 + NO_2) = (1.75 \pm 0.26) \times 10^{-11}\ cm^3\ s^{-1}$ with no apparent temperature dependence in the 251–295 K range. Slagle and Gutman [18] investigated the $CF_2Cl + NO_2$ reaction at 295 K and 1–2 Torr pressure range using photoionization mass spectrometry. They employed infrared multiple-photon-induced decomposition of CF_2Cl_2 as a source of Cl-atoms, which also allowed them to study the $CF_2Cl + NO_2$ reaction rate coefficients, resulting in a room temperature value: $k_{295K}(CF_2Cl + NO_2) = (9.6 \pm 1.9) \times 10^{-12}\ cm^3\ s^{-1}$.

Correlations between reactivity of radicals and different radical properties have been sought to gain understanding of the factors affecting their chemical reactivity. An example of such a procedure is the linear relationship of the electron affinity (EA) of the

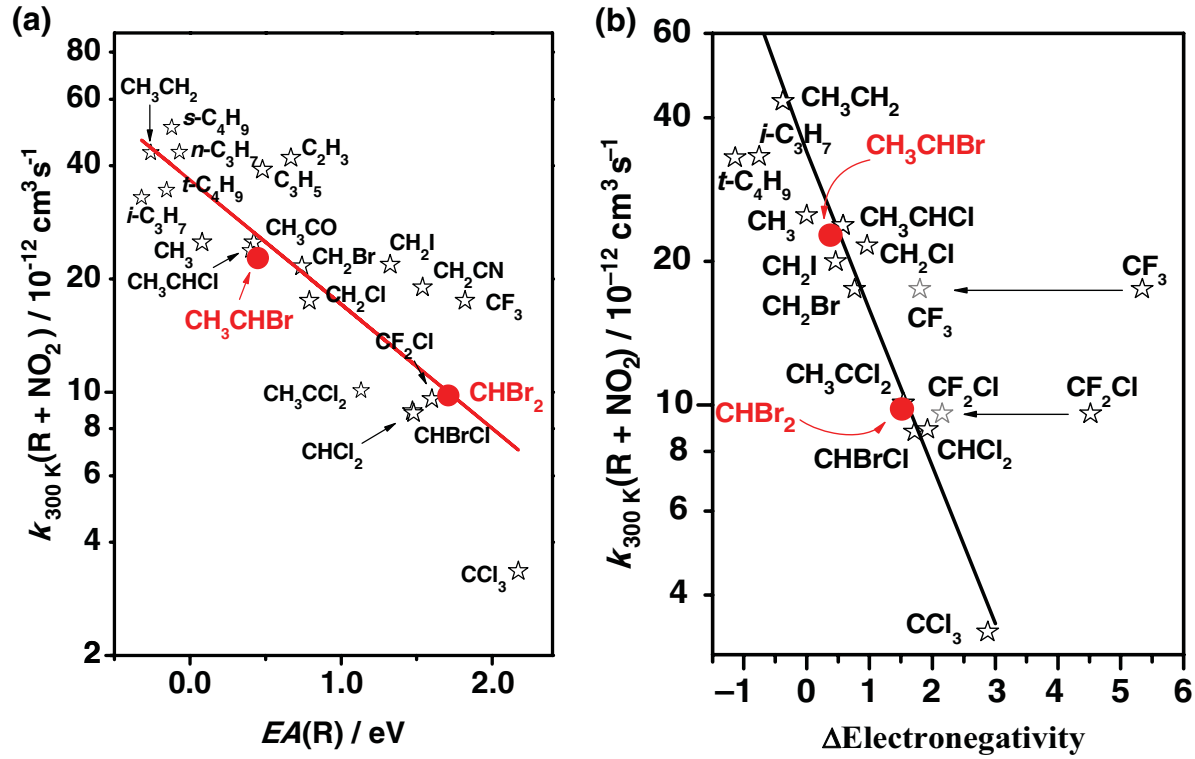

Figure 4 (a) Bimolecular room temperature reaction rate coefficients of current and selected R + NO_2 reactions plotted against the electron affinities of the radicals, EA(R). The rate coefficient of the reaction, displayed on a logarithmic scale, serves as a measure of the radicals' reactivity toward NO_2. Results from this study are presented with circles. The line in the picture is a fit to the data and can be presented by an equation: $k_{300\,K} = (3.66 \times 10^{-11}) \times 10^{-0.33\,EA(R)}$. The selected rate coefficients are from CH_2Cl, $CHCl_2$, and CCl_3 [13]; CH_2Br, CH_2I, and CHBrCl [14]; CH_3CH_2, CH_3CHCl, and CH_3CCl_2 [16]; CF_3 [17]; CF_2Cl and CH_3CO [18]; CH_2CN [27];*n*-C_3H_7, *i*-C_3H_7, *s*-C_4H_9, and *t*-C_4H_9 [40]; CH_3 [51]; C_2H_3 [52]; and C_3H_5 [53]. Electron affinities were taken from [26] except for CH_2I [54], and for CHBrCl [55]. In the case of substituted ethyl radicals, the EA(R) was unavailable and was estimated as $EA(CH_3CHBr) = EA(CH_3CH_2) + (EA(CH_2Br) - EA(CH_3)$. (**b**) A semilogarithmic plot of the room temperature rate coefficients plotted against the ΔElectronegativities of the radicals in the current and selected R + NO_2 reactions. (ΔElectronegativity $= \Sigma X_S - X_H$, where X_H is the hydrogen atom electronegativity and X_S is the substituent atom or group electronegativity). Electronegativities were taken from Pauling [45,46], and an electronegativity value of 1.82 was assigned to a methyl group substituent in accordance with [47]. The line in the picture is a fit to the data omitting the values for fluorinated radicals. The fluorinated radicals share the same relationship when an effective electronegativity value of 2.8 is given to the fluorine atom as a substituent; as was discussed previously along the studies of R + Cl_2 reactions [48,49] and is depicted with horizontal arrows in the picture. The selected rate coefficients were taken from CH_2Cl, $CHCl_2$, and CCl_3 [13]; CH_2Br, CH_2I, and CHBrCl [14]; CH_3CH_2, CH_3CHCl, and CH_3CCl_2 [16]; CF_3 [17]; CF_2Cl [18]; *i*-C_3H_7 and *t*-C_4H_9 [40]; and CH_3 [51]. [Color figure can be viewed in the online issue, which is available at wileyonlinelibrary.com.]

molecular reagent subtracted from the ionization potential of the radical plotted against the logarithm of the room temperature rate coefficient, $\log(k_{300\,K})$ versus (IP(R) − EA(reactant)), used by Paltenghi et al. [43] to correlate the reactivity of alkyl radicals in their reactions with molecular oxygen and ozone. Another example is the ΔElectronegativity scale; an arbitrary scale proposed by Thomas [44] for estimating the electron-withdrawing inductive effects of halogen substituents to carbon 1s IPs calculated by simple summations of the Pauling electronegativities [45,46] of the substituent atoms/groups. To radical kinetics, this semiempirical scale of inductive effects was adapted by Seetula and Gutman [47] to explain the observed differences in the rate coefficients of methyl and halogenated methyl radical reactions with HI. The larger alkyl radicals could be included to the same linear relationship when a group electronegativity value of 1.82 was assigned to the methyl substituent. A similar linear relationship was shown to exist also for the rate coefficients of the R + Cl_2 [48,49] and R + Br_2 [50] reactions.

As noticed by Eskola et al. [13], $\log(k_{300\,K})$ versus (IP(R) − EA(reactant)) does not produce a linear correlation among NO_2 reactions with chlorinated alkyl radicals. Instead it has been observed that the logarithms of the reaction rates correlate with EA of

the radical species; EA(R). $\log(k_{300\,K})$ versus EA(R) and $\log(k_{300\,K})$ versus ΔElectronegativity plots were reproduced here, including also the reactions of the current study. The plots are shown in Figs. 4a and 4b together with selected previously published data. As noted previously [16], polar effects are likely to be important in determining the reactivity differences between the studied R + NO_2 reactions. The lower the charge density in the radical center, that is, the higher the polarity of the radical, (CH_3CHBr > C_2H_5 and $CHBr_2$ > CH_2Br > CH_3) the lower is the reactivity toward NO_2.

Briefly summarizing what has been observed: (i) Electronegative halogen substitution at the radical center decreases the observed R + NO_2 reaction rate coefficients. (ii) Electropositive alkyl substitution has an opposite effect and enhances the rate coefficients. (iii) Br and Cl substitutions in the radical center, in disubstituted methyl, and monosubstituted ethyl radicals have almost the same influence on reaction rates, that is, $k_{300\,K}(CHBr_2 + NO_2) \approx k_{300\,K}(CHBrCl + NO_2) \approx k_{300\,K}(CHCl_2 + NO_2)$ and $k_{300\,K}(CH_3CHCl + NO_2) \approx k_{300\,K}(CH_3CHBr + NO_2)$. (iv) The level of substitution affects the temperature dependence; The more substituted the radical, the stronger is the observed temperature dependence. This is best demonstrated among the measured chlorinated radical reactions, where the n parameter describing T dependence decreases (becomes more negative) as C_2H_5 > CH_3CHCl > CH_3CCl_2 [16] and CH_2Cl > $CHCl_2$ > CCl_3 [13]. (v) Branching of the radical from the α-carbon in comparison with the substituents carbon chain length, that is, i-C_3H_7 versus n-C_3H_7 and t-C_4H_9 versus s-C_4H_9, seems to have a smaller effect on the reactivity of the radical, in contrast what has been observed for R + Cl_2 reactions [48,49], but the results are still inconclusive and to verify them, more data from isomeric radical reactions are needed. Considering the CH_3CHBr radical as an example, the described effects will work on the observed reactivity in the following way: Reactivity is reduced compared with the C_2H_5 radical through halogen substitution at the radical site and enhanced compared with the CH_2Br upon methyl substitution. The reactivity with NO_2 is rather identical in the CH_3CHCl an CH_3CHBr radicals (changing bromine to chlorine substitution) and reduced in comparison with the C_3H_7 and C_4H_9 radicals as CH_3CHBr contains only one alkyl substituent that has the shortest possible carbon chain length.

CONCLUSIONS

The kinetics of $CHBr_2$ and CH_3CHBr radical reactions with NO_2 have been studied in direct experiments under conditions of low pressure (2–6 Torr) and variable temperature (250–480 K). In the $CHBr_2$ + NO_2 reaction, an unexpected product CBr_2O was detected and a mechanism consisting of a four-center transition state was postulated to explain its formation. This pathway is in contrast to the common "alkoxy channel" of R + NO_2 reaction, in which an internally excited nitrite intermediate is formed from R + NO_2 association that breaks into alkoxy radical and nitric oxide. The same kind of mechanism cannot be ruled out from occurring in the CH_3CHBr + NO_2 reaction, but the previous studies and the observed products suggest the formation of an alkoxy radical (CH_3CHBrO) in the reaction. Reactivity of radicals toward NO_2 was briefly discussed and reasoned to be caused by charge density differences at the radical centers.

BIBLIOGRAPHY

1. Quack, B.; Wallace, D. W. R. Global Biogeochem Cycles 2003, 17(1023), 1–27.
2. Carpenter, L. J.; Liss, P. S.; Penkett, S. A. J Geophys Res 2003, 108(D9, 4256), 1–13.
3. Wayne, R. P. Chemistry of Atmospheres, 3rd ed.; Oxford University Press: Cornwall, UK, 2000.
4. Carpenter, L. J.; Liss, P. S. J Geophys Res 2000, 105, 20539–20547.
5. Wever, R.; Tromp, M. G. M.; Krenn, B. E.; Marjani, A.; Van Toi, M. Environ Sci Technol 1991, 25, 446–449.
6. Laturnus, F.; Adams, F. C.; Wiencke, C. Geophys Res Lett 1998, 25, 773–776.
7. Gschwend, P. M.; MacFarlane, J. K.; Newman, K. A. Science 1985, 227, 1033–1035.
8. Itoh, N.; Shinya, M. Marine Chem 1994, 45, 95–103.
9. Theiler, R.; Cook, J. C.; Hager, L. P.; Siuda, J. F. Science 1978, 202, 1094–1096.
10. Schauffler, S. M.; Atlas, E. L.; Blake, D. R.; Flocke, F.; Lueb, R. A.; Lee-Taylor, J. M.; Stroud, V.; Travnicek, W. J Geophys Res 1999, 104, 21513–21535.
11. Bayes, K. D.; Friedl, R. R.; Sander, S. P. J Phys Chem A 2005, 109, 3045–3051.
12. Seetula J. A.; Eskola, A. J. Chem Phys 2008, 351(3), 141–146.
13. Eskola, A. J.; Geppert, W. D.; Rissanen, M. P.; Timonen, R. S.; Halonen, L. J Phys Chem A 2005, 109, 5376–5381.
14. Eskola, A. J.; Wojcik-Pastuszka, D.; Ratajczak, E.; Timonen, R. J Phys Chem A 2006, 110, 12177–12183.
15. Eskola, A. J.; Golonka, I.; Rissanen, M. P.; Timonen, R. S. Chem Phys Lett 2008, 460(4–6), 401–405.
16. Rissanen, M. P.; Eskola, A. J.; Savina, E.; Timonen, R. S. J Phys Chem A 2009, 113(9), 1753–1759.
17. Breheny, C.; Hancock, G.; Morrell, C. Phys Chem Chem Phys 2000, 2, 5105–5112.
18. Slagle I. R.; Gutman, D. J Am Chem Soc 1982, 104, 4741–4752.

19. Eskola A. J.; Timonen, R. S. Phys Chem Chem Phys 2003, 5, 2557–2581.
20. Eskola, A. J.; Wojcik-Pastuszka, D.; Ratajczak, E.; Timonen, R. S. Phys Chem Chem Phys 2006, 8, 1416–1424.
21. Zou, P.; Shu, J.; Sears, T. J.; Hall, G. E.; North, S. W. J Phys Chem A 2004, 108, 1482–1488.
22. Lee, Y. R.; Chen, C. C.; Lin, S. M. J Chem Phys 2003, 118, 10494–10501.
23. Sander, S. P.; Friedl, R. R.; Ravishankara, A. R.; Golden, D. M.; Kolb, C. E.; Kurylo, M. J.; Molina, M. J.; Moortgat, G. K.; Keller-Rudek, H.; Finlayson-Pitts, B. J.; Wine, P. H.; Huie, R. E.; Orkin, V. L. Chemical Kinetics and Photochemical Data for Use in Stratospheric Modelling: Evaluation Number 15, Publication 06-2: National Aeronautics and Space Administration, Jet Propulsion Laboratory, California Institute of Technology, Pasadena, CA, 2006.
24. Borrell, P.; Cobos, C. J.; Luther, K. J Phys Chem 1988, 92, 4377–4383.
25. Harwood, M. H.; Jones, R. L. J Geophys Res 1994, 99(D11), 22955–22964.
26. Linstrom, P. J.; Mallard, W. G. NIST Chemistry Webbook, NIST Standard Reference Database Number 69, June 2005: National Institute of Standards and Technology: Gaithersburg MD. Available at: http://webbook.nist.gov. Accessed January 2012.
27. Park, J. Y.; Gutman, D. J Phys Chem 1983, 87, 1844–1848.
28. Gray, P. Trans Faraday Soc 1955, 51, 1367–1374.
29. Ballod, A. P.; Shtern, V. Ya. Russ Chem Rev 1976, 45, 721–737. (Usp Khim 1976, 45, 1428, in Russian.)
30. Orlando, J. J.; Tyndall, G. S.; Wallington, T. J.; Dill, M. Int J Chem Kin 1996, 28, 433–442.
31. Orlando, J. J.; Tyndall, G. S.; Wallington, T. J. Chem Rev 2003, 103, 4657–4689.
32. Drougas, E.; Kosmas, A. M. Chem Phys 2005, 310, 249–256.
33. Chase, M. W., Jr. NIST-JANAF Thermochemical Tables, 4th ed.; J Phys Chem Ref Data, Monograph 9, 1998, 1–1951.
34. Dunning, B. K.; Pritchard, H. O. J Chem Thermodyn 1972, 4, 213–218.
35. Xu, D.; Francisco, J. S.; Huang, J.; Jackson, W. M. J Chem Phys 2002, 117, 2578–2585.
36. Reed, R. I.; Snedden, W. J Chem Soc, Faraday Trans 1958, 54, 301–307.
37. Sugawara, K.; Nakanaga, T.; Takeo, H.; Matsumura, C. J Phys Chem 1989, 93, 1894–1898.
38. Drougas, E.; Kosmas, A. M. Chem Phys Lett 2003, 379, 297–304.
39. Orlando J. J.; Tyndall, G. S. J Phys Chem A 2002, 106, 312–319.
40. Rissanen, M. P.; Arppe, S. L.; Eskola, A. J.; Tammi, M. M.; Timonen, R. S. J Phys Chem A 2010, 114(14), 4811–4817.
41. Osborn, D. L.; Zou, P.; Johnsen, H.; Hayden, C. C.; Taatjes, C. A.; Knyazev, V. D.; North, S. W.; Peterka, D. S.; Ahmed, M.; Leone, S. R. Rev Sci Instrum 2008, 79(104103), 1–10.
42. Wiberg, K. B.; Crocker, L. S.; Morgan, K. M. J Am Chem Soc 1991, 113, 3447–3450.
43. Paltenghi, R.; Ogryzlo, E. A.; Bayes, K. D. J Phys Chem 1984, 88, 2595–2599.
44. Thomas, T. D. J Am Chem Soc 1970, 92, 4184–4189.
45. Pauling, L. Nature of the Chemical Bond, 3rd ed.; Cornell University Press: Ithaca, NY, 1960; pp 88–95.
46. Allred, A. L. J Inorg Nucl Chem 1961, 17, 215–221.
47. Seetula, J. A.; Gutman, D. J Phys Chem 1991, 95, 3626–3630.
48. Seetula, J. A.; Gutman, D.; Lightfoot, P. D.; Rayes, M. T.; Senkan, S. M. J Phys Chem 1991, 95, 10688–10693.
49. Rissanen M. P.; Eskola, A. J.; Timonen, R. S. J Phys Chem A 2010, 114(14), 4805–4810.
50. Timonen, R. S.; Seetula, J. A.; Niiranen, J.; Gutman, D. J Phys Chem 1991, 95, 4009–4014.
51. Yamada, F.; Slagle, I. R.; Gutman, D. Chem Phys Lett 1981, 83, 409–412.
52. Geppert, W. D.; Eskola, A. J.; Timonen, R. S.; Halonen, L. J Phys Chem A 2004, 108, 4232–4238.
53. Slagle, I. R.; Yamada, F.; Gutman, D. J Am Chem Soc 1981, 103, 149–153.
54. Born, M.; Ingemann, S.; Nibbering, N. M. M. J Am Chem Soc 1994, 116, 7210–7217.
55. Born, M.; Ingemann, S.; Nibbering, N. M. M. Int J Mass Spectrom Ion Processes 2000, 194, 103–113.